Nanoscale

COMMUNICATION

View Article Online
View Journal | View Issue

Cite this: *Nanoscale*, 2020, **12**, 6603

Received 29th November 2019,
Accepted 2nd March 2020

DOI: 10.1039/c9nr10145d

rsc.li/nanoscale

Radio- and nano-chemistry of aqueous Ga(III) ions anchored onto graphene oxide-modified complexes†

S. Sarpaki,‡[a] F. Cortezon-Tamarit,‡[a] S. R. M. M. de Aguiar,‡[a] R. M. Exner,[a] D. Divall,[a] R. L. Arrowsmith,[a] H. Ge,[a] F. J. Palomares,[b] L. Carroll,[c] D. G. Calatayud,[d] S. J. Paisey,[e] E. O. Aboagye[f] and S. I. Pascu*[a]

The gallium-68 radiolabelling of new functional graphene oxide composites is reported herein along with kinetic stability investigations of the radio-nanohybrids under different environments and insights into their surface characteristics by SEM and XPS. The present work highlights the potential of graphene oxides as nanocarriers for small molecules such as bis(thiosemicarbazonato) complexes to act as multifunctional platforms for rapid and effective radioimaging agent incorporation.

The research field of nanotechnology has been continuously advancing over the past 20 years on account of the unique physicochemical properties of emergent nanostructured materials including graphene and functional graphenes. This has allowed for innovative applications in broad areas of biomedical sciences and already provides potential solutions to many of the current scientific and technological challenges such as those of new developments in biosensing as well as in nanomedicine design and testing. In this context, graphene and graphene oxide have shown great potential in the development of a broad range of biomedical applications.[1,2] Due to graphene oxide's improved water solubility and superior biocompatibility in comparison to graphene or other nanoparticles (*e.g.* metallic nanoparticles), its use as a nanocarrier for drug/gene delivery[3–7] or as a probe in molecular imaging is being explored.[6–11] Currently, functional graphenes and their covalent and non-covalent functionalised derivatives have been investigated as potential nanoplatforms for a variety of imaging techniques, such as magnetic resonance imaging (MRI),[8,12–14] fluorescence,[8,15–17] positron emission tomography (PET) and photoacoustic imaging.[8,18–20] In addition, the combination of different imaging modalities on the same nanocomposite has been explored.[8,21,22]

Several recent studies show that graphene oxide (GO) nanocomposites can be conjugated with polyethylene glycol (PEG) or small chelating molecules (*e.g.* 1,4,7-triazacyclononane-1,4,7-trisacetic acid, deferoxamine, *etc.*) and, in turn, radiolabelled with various radioisotopes (*e.g.* iodine-131, gallium-66, gallium-68, copper-64).[8,23–25] for their use in nuclear imaging.

Recently Cai *et al.* suggested that the chelator-free labelling of GO nanocomposites with copper-64 is possible, allowing for the facile synthesis of new radio-nanocomposites with high kinetic stability.[26,27] These radiolabelling processes can be carried out under mild conditions and rely on the interaction between the transition metal and π electrons and oxygen functionalities present on GO surface. Although this approach offers an attractive alternative for the radiolabelling of GO, only a few examples have been reported using copper-64 or fluorine-18.[26–28]

Despite the progress achieved so far, there are still many synthetic limitations to be resolved in order to develop new materials that are not only biocompatible but also stable, allowing for the development of new versatile contrast agents. In this sense, the large surface area of sp^2-bound carbon in graphene oxide nanocomposites added to the presence of oxygen functionalities become a crucial factor for the functionalisation of graphene covalently, or non-covalently *via* π–π interactions, hydrogen bonding or van der Waals forces.

In this work, we demonstrated the feasibility of graphene oxide as a potential chelator-free imaging contrast in [^{68}Ga]Ga

[a]*Department of Chemistry, University of Bath, Claverton Down, BA2 7AY Bath, UK. E-mail: s.pascu@bath.ac.uk*
[b]*Department of Nanostructures and Surfaces, Instituto de Ciencia de Materiales de Madrid – CSIC, Sor Juana Inés de la Cruz 3, Madrid, 28049, Spain*
[c]*Department of Radiology & Radiological Science, Johns Hopkins, 601 N Caroline St, Baltimore, MD 21205, USA*
[d]*Department of Electroceramics, Instituto de Cerámica y Vidrio – CSIC, Kelsen 5, Madrid, 28049, Spain*
[e]*Wales Research and Diagnostic PET Imaging Centre, School of Medicine, Cardiff University, Cardiff, UK*
[f]*Department of Surgery and Cancer, Faculty of Medicine, Commonwealth Building, Hammersmith Campus, Imperial College London, Du Cane Road, London, W12 0NN, UK*
†Electronic supplementary information (ESI) available: Detailed Experimental section, spectroscopic and materials characterisations, radiolabelling, cellular imaging and cytotoxicity assays. See DOI: 10.1039/c9nr10145d
‡These authors contributed equally to the work.

(III)-radiolabelling with excellent radiochemical yields. The prepared graphene oxide nanocomposites also incorporated functional bis(thiosemicarbazonato) metal complexes and tested the applicability of these derivatives *in vitro* paving the way towards the potential application in PET imaging of graphene oxide-based multimodality imaging nanoprobes.

The unsymmetrical bis(thiosemicarbazonato) zinc complex (**2**), synthesised as described in Fig. 1 and ESI,† was selected for the potential enhancement of the GO-based radionanocomposite properties as related/similar compounds have shown inherent hypoxia selectivity.[29,30] In this case, a free amino group incorporated in the ligand framework at the exocyclic N(H) in **2** opens the way for future straightforward bioconjugations. The synthesis of gallium bis(thiosemicarbazonato) complex was additionally carried out: the non-radiolabelled and radiolabelled gallium(III) complexes (**3** and **[^{68}Ga]-3**) were prepared *via* an optimised, transmetallation protocol from the corresponding zinc complex precursor (**2**) allowing for a reduction in reaction times and increased reaction yields (Tables S3 and S4, ESI†). The radiochemical purity of the gallium-68 complex was demonstrated by HPLC and radio-HPLC: Fig. 2(A) shows a comparison of the relevant traces of Compound **3** and the corresponding species **[^{68}Ga]-3**.

The aqueous gallium(III) and [^{68}Ga]gallium(III) ions were subsequently incorporated into two different nanoparticulate systems: a simple **GO** framework and a **GO**-based hybrid incorporating a molecular bis(thiosemicarbazonato) zinc complex (**2@GO**), as described in Fig. 1(B). The gallium-tagged nanocomposites were successfully prepared by mixing a GO suspension in DMSO (2 mg mL^{-1}) with $GaCl_3$ in a 4 : 1 ethanol : sodium acetate buffer solution (pH = 4.5) at 95 °C for 45 minutes. Next the [^{68}Ga]Ga(III) radiolabelling was achieved following the analogous procedure employed for the non-radioactive counterparts. This resulted in the isolation of the two radioactive hybrids, or nanocomposites, denoted **[^{68}Ga]Ga@GO** and **[^{68}Ga]Ga-2@GO**. The source of the [^{68}Ga]$GaCl_3$ (aq.) *i.e.* whether it was generator *vs.* cyclotron produced did not appear to play a crucial role in the formation of a nanohybrid: the labelling was successful with gallium-68 produced by a cyclotron *via* the ^{89}Zn(p,n)^{68}Ga reaction in aqueous solution, or eluted through a [^{68}Ge]/[^{68}Ga] generator, in both cases the impurities present after extractions appeared to play a negligible role in the immobilisation of radioactive species within the support. All the reactions were monitored using radioactive instant thin layer chromatography (radio-iTLC). The radio-iTLC, based on the percentage of activity detected on the baseline by paper chromatography (Whatman 3MM), suggested that after 45 min the radiochemical conversion (RCCs) for both [^{68}Ga]-labelled GO nanocomposites was higher than 99% as single radioactive species were detected for each Radio-iTLC run (Fig. 2B and Fig. S65 of ESI†). The radiochemical yield of crude gallium-68 nanocomposites was calculated to be notably high and varied between the different nanocomposites used from 98 ± 4.6% to 99.7 ± 0.74%. It can be assumed that labelling was enabled by interactions of the oxophilic Ga(III) ion

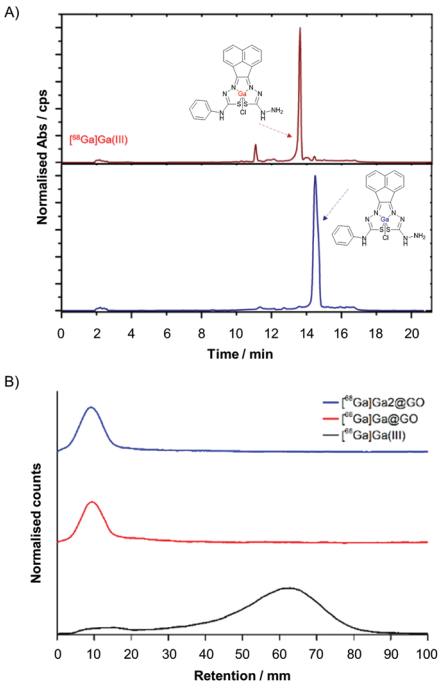

Fig. 2 (A) HPLC and radio-HPLC traces for complexes **3** (blue), and **[^{68}Ga]-3** (red). (B) Radiochemical data for the [^{68}Ga]-radiolabelling of GO nanocomposites. Small impurities at 11 min are assignable to protonation and/or Ga–Cl/Ga–OH exchanges in water. Radio-iTLC of **[^{68}Ga]Ga@GO** and **[^{68}Ga]Ga-2@GO** (C18 paper TLC, mobile phase: 0.35 M EDTA).

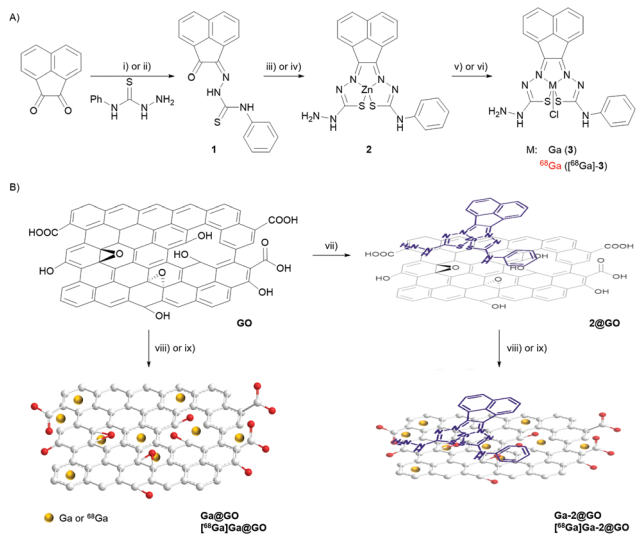

Fig. 1 (A) Synthetic procedure for complexes **2** and **3**. (i) EtOH, HCl, reflux, 2 h; (ii) EtOH, HCl, μW 90 °C, 10 min; (iii) $Zn(OAc)_2$, $(NH_2NH)_2CS$, CH_3COOH, 120 °C, 28 h; (iv) $Zn(OAc)_2$, $(NH_2NH)_2CS$, EtOH, HCl, μW 150 °C, 1 h 46 min; (v) $GaCl_3$, MeOH, reflux, 6 h; (vi) [^{68}Ga]$GaCl_3$, MeOH, NaOAc, 95 °C, 45 min. (B) Formation of nano-composites denoted Ga@GO, Ga-2@GO and of radiolabelled analogues. (vii) Complex **2**, $NaHCO_3$, reflux, 2.5 h; (viii) $GaCl_3$, $NaHCO_3$, 100 °C, 2.5 h; (ix) [^{68}Ga]$GaCl_3$, $NaHCO_3$, 95 °C, 45 min.

with the surface functionalities of GO, although transition metal-π electron interactions based on the electron transfer between Ga(III) cations, well-known hard/intermediate Lewis acids and π electron density on the surface of GO, may further facilitate this binding.

The kinetic stability of both non-radiolabelled (**Ga@GO** and **Ga-2@GO**) and radiolabelled nanocomposites (**[^{68}Ga]Ga@GO** and **[^{68}Ga]Ga-2@GO**) was evaluated under various conditions. For the kinetic stability tests of the non-radiolabelled complexes, (**Ga@GO** and **Ga-2@GO**) UV-visible absorption spectroscopy was employed. Specifically, 2 mg mL^{-1} concentration of the assay agent (complex **Ga@GO** or **Ga-2@GO**) dispersed in DMSO was used. Dispersions of assay agents in 1 : 1 DMSO : H_2O mixtures were prepared, and the assays were carried out by incubating the samples at 37 °C using citric acid, PBS, EDTA and DFO. Both complexes were found to be sufficiently stable in the timescale of an imaging experiment with respect to decomposition in a mixture of DMSO and several aqueous buffers, which are of relevance to standard cellular imaging assays. Whilst there were no changes observed in the UV/Vis spectra after 30 minutes of incubation, some slight changes were observed after 24 hours of incubation (Fig. S52 in ESI†). Moreover, on account of the short half-life ($t_{1/2}$) of [^{68}Ga]Ga(III) (68 minutes), the kinetic stability of the radiolabelled compounds was tested after incubation at 37 °C for 60 and 120 minutes. It was found that the stability profile of the radiolabelled complex was high with >98% of the radiolabelled GO nanocomposites remaining intact during incubation in biological media (*e.g.* PBS, mouse plasma) at a volume ratio of 1 : 1 of the radiolabelled GO nanocomposites to biological media. On the other hand, the stability in EDTA decreased compared to biological media with only >65% remaining intact after one hour, which might be caused by the strong ability of EDTA to bind gallium(III).[31] Fig. 3 shows a bar graph representation summarising the stability assay results for the **[^{68}Ga]Ga@GO** and **[^{68}Ga]Ga-2@GO** nanocomposites. Interestingly, the ananlogous methodology could be extrapolated to the chelator-free [^{89}Zr]Zr-labelling of **GO** [ESI†]. The incorporation of (cyclotron-produced) aqueous ^{89}Zr(IV) into the **2@GO** hybrid was also attempted to test the hypothesis that the Lewis acidity and oxophilicity of Zr(IV) would lead to specific radiolabelling. Further investigations of the potential radiolabelling using [^{89}Zr]Zr(IV) (aqueous ions, frequently highlighted as a mixture of colloidal oxo-zirconium ions) in the presence of the well-known zirconium chelator, the siderophore-like deferoxamine (DFO) derivative, were carried out hereby. The radiolabelled [^{89}Zr]ZrDFO was treated in turn with the **GO** and **2@GO** nanocomposites and a 70% radio-incorporation of this complex was observed. We hypothesise that this could be caused by non-covalent binding between GO nanocomposites and DFO. Our experiments did not indicate a strong kinetic stability of the resulting ^{89}Zr(IV)-tagged radio-nanohybrids and did not confirm the strong binding of the zirconium-89 to GO in the absence of the established chelator deferoxamine (DFO) (ESI, Fig. S40†).

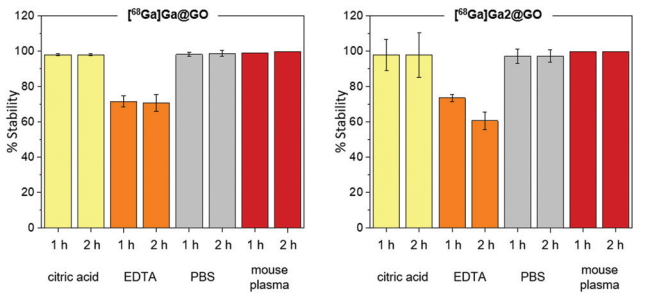

Fig. 3 Kinetic stability tests: **[^{68}Ga]Ga@GO** (left) and **[^{68}Ga]Ga-2@GO** (right) Nanocomposites were exposed up to 2 h to challenges under various incubation conditions described in ESI.† Error bar stands for standard error (±SE), calculated from three independent, repeated, measurements.

To aid our understanding into the interaction within the GO nanocomposites and gallium species on the nanoscale, further analysis through TEM, SEM and EDX in the 'cold' Ga (III) chemistry was applied. The electron microscopy images of the corresponding 'cold' compounds indicated some level of aggregation of the Ga^{+3} ions and of the **Ga-2** complex on the surface or between the layers of the GO flakes, suggesting an interaction in solution (ESI†). The EDX mapping of **Ga-2@GO** showed a high binding affinity of Ga(III) on the GO surface, supporting the hypothesis that when bis(thiosemicarbazonato) Zn(II) complex is incorporated non-covalently within the GO layers, the normally straight-forward transmetallation Zn(II)/Ga (III) reaction[30] seems less favourable (Fig. 5). In order to confirm the bonding condition of gallium and surface functionalizations of graphene oxide XPS measurements were performed. In survey scans, the expected emissions from core level peaks can be observed (C 1s, N 1s, Zn 2p, Cl 2p, O 1s and Ga 3p and 3d. These were present in samples **Ga (3)** and **Ga-2@GO**, and C 1s, Cl 1s, O 1s and Ga 3p and 3d for **Ga@GO**. For chemical analysis and comparison purposes, N 1s, Zn 2p and Ga 3d levels were selected (Fig. 6). Interestingly, Fig. 6(a) depicts the XPS emission attesting the presence of traces of Zn: from the Zn 2p core level, whose binding energy and core level splitting values confirm the presence of Zn^{2+} in both Ga (**3**) and **Ga-2@GO** samples. The existence of Zn in the sample Ga (**3**) can be ascribed to the transmetallation reaction, and therefore the presence of small amounts of the Zn thiosemicarbazonato precursor, which are undetectable through analytical techniques such as HPLC, NMR or mass spectrometry. Fig. 6(b) shows the XPS spectra corresponding to the N 1s core level: for the samples **Ga (3)** and **Ga-2@GO** a peak at *ca.* 399 eV can be observed corresponding to the emission from N of the thiosemicarbazonato complexes; correspondingly no N-related signal was detected for the **Ga@GO** sample due to the absence of the thiosemicarbazato complexes. In addition, for all samples a Cl 2p peak (Fig. S50, ESI†) corresponding to the Cl–Ga bond was readily seen. The sample **Ga@GO** shows, as expected, the highest Cl percentage, due to the use of $GaCl_3$ as the Ga(III) source. The obtained

data confirms the presence of Ga(III) ions in all samples (Fig. 6c). Both the binding energy position of the Ga 3d photoemission peak (*ca.* 21 eV) and the LMM Auger transitions (Fig. S50 ESI†), shifted 3.0 eV and 6.0 eV with respect to the values for metallic Ga, respectively, confirming the presence of Ga^{3+} (ESI†). A detailed analysis of the Ga 3d energy region provides more information of its chemical state. At first, subtle line shape asymmetry is observed on the low binding energy side, which might be indicative of an additional emission associated to a lower chemical state. Therefore, core level fit has been performed considering components from O 2s, Ga 3d, Cl 3s, S 3s and Zn 3d signals present in that energy region. The deconvolution results are displayed in Fig. 6(d), (e) and (f) for all the samples. In addition to the main contribution attributed to Ga^{3+}, a minor component assignable to Ga–OH exists (denoted Ga^{+1} in the Fig. 6), suggesting the possible presence of Ga–OH-graphene oxide surface conjugations for **Ga@GO** and **Ga-2@GO** and of $Ga(OH)_3$ for **Ga (3)**.[33–36] This is an unprecedented account into the behaviour of gallium ions in presence of graphene oxides and also shows an insight for the first time into the Zn(II)/Ga(III) transmetallation from XPS spectroscopy.

Furthermore, the cellular uptake of the complexes **2** and **3** and the corresponding nanocomposite **2@GO** in living PC-3 cancer cells was investigated by laser confocal fluorescence

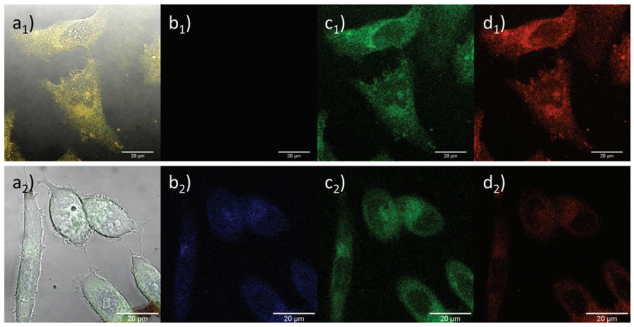

Fig. 4 Single photon laser scanning confocal fluorescence imaging of **2** (a_1–d_1) in living HeLa cells (100 μM, 37 °C, 15 min incubation in RPMI-0.5% DMSO) and **2@GO** (a_2–d_2) in living PC-3 cells (10 μg mL^{-1}, 37 °C, 15 min incubation in RPMI-0.5% DMSO). (a_{1-2}) Overlay of DIC, blue, green and red channels; (b_{1-2}) blue channel, λ_{exc} 405 nm, λ_{em} 420–480 nm; (c_{1-2}) green channel, λ_{exc} 488 nm, λ_{em} 515–530 nm; (d_{1-2}) red channel, λ_{exc} 561 nm, λ_{em} 615–650 nm. Scale bar: 20 μm.

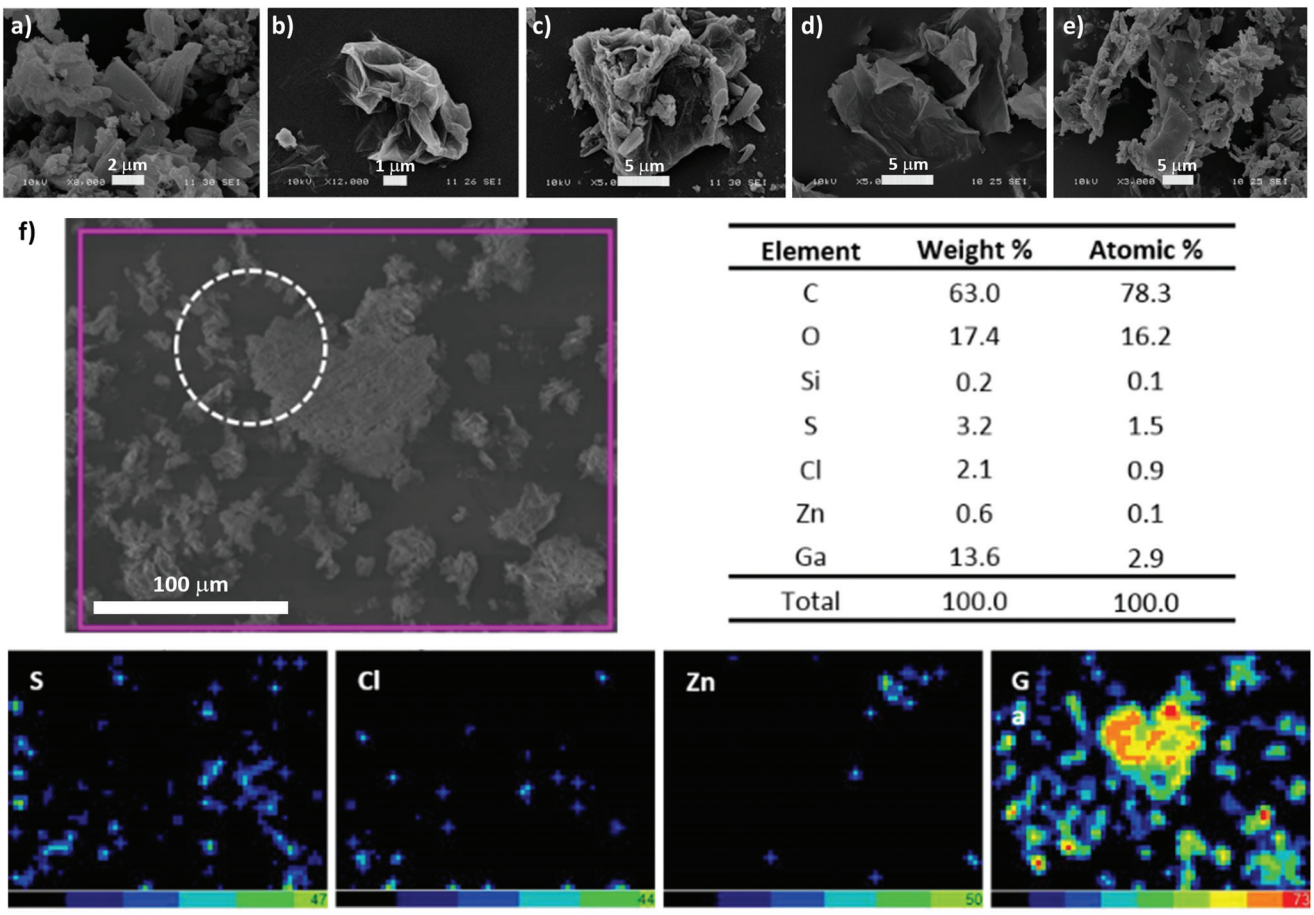

Element	Weight %	Atomic %
C	63.0	78.3
O	17.4	16.2
Si	0.2	0.1
S	3.2	1.5
Cl	2.1	0.9
Zn	0.6	0.1
Ga	13.6	2.9
Total	100.0	100.0

Fig. 5 Scanning Electron Microscopy (SEM): micrographs and corresponding EDX analysis of complexes and nanocomposites. (a) Complex **2**; (b) **GO**; (c) **2@GO**; (d) **Ga@GO** and (e) **Ga-2@GO**. Scale bars: (a) 2 μm, (b) 1 μm, (c), (d) and (e) 5 μm. (f) SEM image and corresponding EDX elemental analysis and EDX mapping image (S, Cl, Zn, Ga) of **Ga-2@GO** nanocomposite.

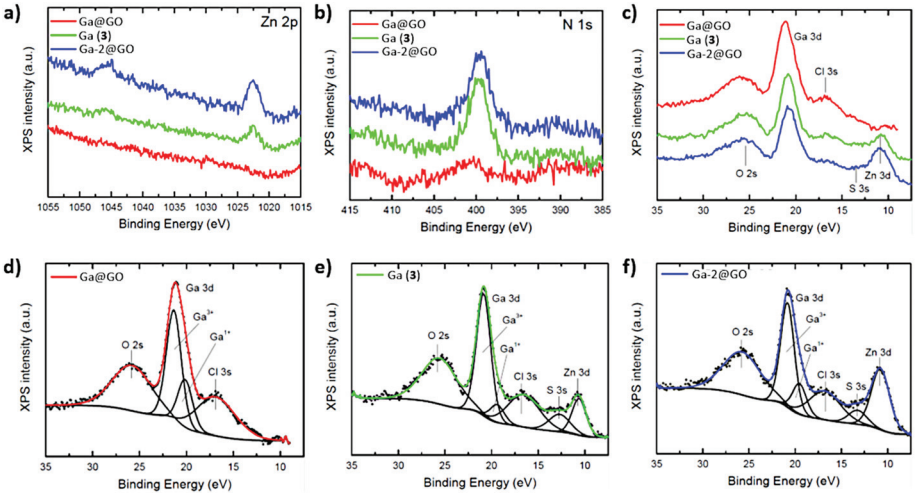

Fig. 6 XPS spectra of core levels (a) Zn 2p, (b) N 1s, (c) Ga 3d. (d) Ga 3d energy region for the Ga@GO sample with a fit of a Ga^{3+}, **3** Ga–O singlet, Ga^{1+}, and Ga–Cl, (e) and (f) same scenario than (d) but for the Ga (**3**) and Ga-2@GO samples.

microscopy (ESI†). Whilst these species display weak fluorescence emission, consistent with all related studies on metallated bis(thiosemicarbazonato) species, this was sufficient to perform *in vitro* imaging (Fig. 4 and ESI†) by confocal fluorescence microscopy. Complex **2** exhibited a stronger fluorescence emission when localised within the cytoplasm of living HeLa, PC-3 and MCF-7 cell lines, in line with previously reported observations.[29] Interestingly, complex **3** shows a stronger fluorescence emission intensity under hypoxic conditions (ESI†) consistent with previous findings on the hypoxia selectivity of this family of gallium compounds supported on rigid N/S ligand frameworks.[29,30] Cellular cytotoxicity investigations performed on the non-radiolabelled compounds in PC-3 and EMT-6 cancer cell lines (ESI†) confirmed the low toxicity of the synthesised graphene oxide nanocomposites in these particular cell lines, being suitable candidates as synthetic scaffolds for anchoring imaging agents. Crystal violet assays were carried out in the PC-3 and EMT-6 cancer cell lines. All the GO composites investigated had low to minimum toxicity under the selected experimental conditions[11] and in the case of the molecular compounds, their IC_{50} values are in line with previous investigations into this family of bis(semithiocarbazonato) complexes[29] (Fig. S24–S29, ESI†). Functional graphene oxides are now well known to be excreted *in vivo* through the kidney and the gut:[32] lack of cellular toxicity reinforce the possibility of sustainable and safe radioactivity entrapment by metal compounds anchored onto the 2D layers of graphene oxides.

Conclusions

In conclusion, we report hereby the chelator-free radiolabelling of GO nanocomposites with gallium-68. For the first time, GO nanocomposites were directly radiolabelled with aqueous $[^{68}Ga]GaCl_3$ through non-covalent interactions without the need to use a chelator. Almost quantitative radioactivity incorporation was achieved in record times of under 1 h. The functionalisation of the GO flakes with functional molecules was demonstrated by using a Zn(II)-based bis(thiosemicarbazonato) metal complex with enhanced fluorescence and provided potential selectivity towards hypoxic tissues. The ease of functionalisation may facilitate the application of GO nanocomposite as synthetic platforms towards biomedical/bioimaging applications. Our hypotheses for the nanohybrid formation were verified by utilising different types of microscopy (optical and SEM) and chemical analysis of the material and resultant complexes at the local scale (nano) and micro-scale. Furthermore, XPS measurements shed light onto the nature of the emerging bonding interactions and confirmed our successful developments in the rapid assembly of new radioactive nanohybrids based on gallium ions, directly or as complex ions incorporating the Ga/S/N cores. The kinetic stability of the complexes proved to be excellent in PBS or serum in the timescale of an imaging experiment. In addition, crystal violet assays were carried out on the non-radiolabelled complexes indicating high cell viability, rendering them appropriate candidates as imaging agents as well as of interest for radioactive waste-water remediation and storage for longer lived isotopes. These findings open up new vistas for radio-nanomaterials research avenues and bring about a new focus on the future use of affordable, water-dispersible and biocompatible 2D-materials such as graphene oxides as radio-nanomedicine building blocks.

Conflicts of interest

There are no conflicts to declare.

Acknowledgements

The S. I. P. group thanks the Centre for Doctoral Training in Sustainable Chemical Technologies (EP/L016354/1). SIP also acknowledges the EU funding through the ERC for the Consolidator Grant O2SENSE (617107, 2014–2020). The authors thank EPSRC National Service for Mass Spectrometry at Swansea and for data collection. We thank Professor Stan Botchway for training in confocal fluorescence microscopy and Professor Jon Dilworth for helpful discussions in the radiochemistry of bis(thiosemicarbazones). The EOA group acknowledges support from Imperial College NIHR Biomedical Research Centre, Cancer Research UK (C2536/A16584) and the UK Medical Research Council (MR/J007986/1). D. G. C. also acknowledges the Fundación General CSIC (ComFuturo Program) for the financial support and F. J. P. the Spanish Ministry of Economy and Competitiveness (MINECO) (MAT2016-80394-R).

References

1 X. Zhu, Y. Liu, P. Li, Z. Nie and J. Li, *Analyst*, 2016, **141**, 4541–4553.
2 D. G. Calatayud, F. Cortezon-Tamarit, B. Mao, V. Mirabello and S. I. Pascu, in *Handbook of Graphene*, 2019, pp. 469–505.
3 X. Sun, Z. Liu, K. Welsher, J. T. Robinson, A. Goodwin, S. Zaric and H. Dai, *Nano Res.*, 2008, **1**, 203–212.
4 H. Bao, Y. Pan, Y. Ping, N. G. Sahoo, T. Wu, L. Li, J. Li and L. H. Gan, *Small*, 2011, **7**, 1569–1578.
5 L. Zhang, J. Xia, Q. Zhao, L. Liu and Z. Zhang, *Small*, 2010, **6**, 537–544.
6 M. Orecchioni, R. Cabizza, A. Bianco and L. G. Delogu, *Theranostics*, 2015, **5**, 710–723.
7 K. Yang, S. Zhang, G. Zhang, X. Sun, S.-T. Lee and Z. Liu, *Nano Lett.*, 2010, **10**, 3318–3323.
8 J. A. Tyson, D. G. Calatayud, V. Mirabello, B. Mao and S. I. Pascu, *Adv. Inorg. Chem.*, 2016, **68**, 397–440.
9 G. Gollavelli and Y. C. Ling, *Biomaterials*, 2012, **33**, 2532–2545.
10 X. Huang, S. Lee and X. Chen, *Am. J. Nucl. Med. Mol. Imaging*, 2011, **1**, 3–17.
11 J. A. Tyson, V. Mirabello, D. G. Calatayud, H. Ge, G. Kociok-Köhn, S. W. Botchway, G. D. Pantoş and S. I. Pascu, *Adv. Funct. Mater.*, 2016, **26**, 5641–5657.
12 L. Chen, L. Zhang, J. Bao, J. Zhang, C. Li, Y. Xia, X. Huang and J. Wang, *Gut*, 2013, **62**, 1520–1521.
13 S. Wang, Q. Zhang, X. F. Luo, J. Li, H. He, F. Yang, Y. Di, C. Jin, X. G. Jiang, S. Shen and D. L. Fu, *Biomaterials*, 2014, **35**, 9473–9483.
14 W. Chen, P. Yi, Y. Zhang, L. Zhang, Z. Deng and Z. Zhang, *ACS Appl. Mater. Interfaces*, 2011, **3**, 4085–4091.
15 M.-L. Chen, J.-W. Liu, B. Hu, M.-L. Chen and J.-H. Wang, *Analyst*, 2011, **136**, 4277–4283.
16 P. S. Wate, S. S. Banerjee, A. Jalota-Badhwar, R. R. Mascarenhas, K. R. Zope, J. Khandare and R. D. K. Misra, *Nanotechnology*, 2012, **23**, 415101.
17 J. Ge, M. Lan, B. Zhou, W. Liu, L. Guo, H. Wang, Q. Jia, G. Niu, X. Huang, H. Zhou, X. Meng, P. Wang, C. S. Lee, W. Zhang and X. Han, *Nat. Commun.*, 2014, **5**, 4596.
18 H. Hong, K. Yang, Y. Zhang, J. W. Engle, L. Feng, Y. Yang, T. R. Nayak, S. Goel, J. Bean, C. P. Theuer, T. E. Barnhart, Z. Liu and W. Cai, *ACS Nano*, 2012, **6**, 2361–2370.
19 K. Yang, L. Feng, H. Hong, W. Cai and Z. Liu, *Nat. Protoc.*, 2013, **8**, 2392–2403.
20 S. Shi, K. Yang, H. Hong, H. F. Valdovinos, T. R. Nayak, Y. Zhang, C. P. Theuer, T. E. Barnhart, Z. Liu and W. Cai, *Biomaterials*, 2013, **34**, 3002–3009.
21 G. Gollavelli and Y.-C. Ling, *Biomaterials*, 2014, **35**, 4499–4507.
22 S. H. Hu, Y. W. Chen, W. T. Hung, I. W. Chen and S. Y. Chen, *Adv. Mater.*, 2012, **24**, 1748–1754.
23 J. Lamb, E. Fischer, M. Rosillo-Lopez, C. G. Salzmann and J. P. Holland, *Chem. Sci.*, 2019, **10**, 8880–8888.
24 H. Hong, K. Yang, Y. Zhang, J. W. Engle, L. Feng, Y. Yang, T. R. Nayak, S. Goel, J. Bean, C. P. Theuer, T. E. Barnhart, Z. Liu and W. Cai, *ACS Nano*, 2012, **6**, 2361–2370.
25 H. Hong, Y. Zhang, J. W. Engle, T. R. Nayak, C. P. Theuer, R. J. Nickles, T. E. Barnhart and W. Cai, *Biomaterials*, 2012, **33**, 4147–4156.
26 S. Shi, C. Xu, K. Yang, S. Goel, H. F. Valdovinos, H. Luo, E. B. Ehlerding, C. G. England, L. Cheng, F. Chen, R. J. Nickles, Z. Liu and W. Cai, *Angew. Chem., Int. Ed.*, 2017, **56**, 2889–2892.
27 S. Shi, C. Xu, K. Yang, R. Nickles, Z. Liu and W. Cai, *J. Nucl. Med.*, 2016, **57**, 392.
28 S. C. Jang, S. M. Kang, J. Y. Lee, S. Y. Oh, A. T. E. Vilian, I. Lee, Y. K. Han, J. H. Park, W. S. Cho, C. Roh and Y. S. Huh, *Int. J. Nanomed.*, 2018, **13**, 221–234.
29 I. S. Alam, R. L. Arrowsmith, F. Cortezon-Tamarit, F. Twyman, G. Kociok-Kohn, S. W. Botchway, J. R. Dilworth, L. Carroll, E. O. Aboagye and S. I. Pascu, *Dalton Trans.*, 2016, **45**, 144–155.
30 F. Cortezon-Tamarit, S. Sarpaki, D. G. Calatayud, V. Mirabello and S. I. Pascu, *Chem. Rec.*, 2016, **16**, 1380–1397.
31 D. J. Hnatowich, *J. Nucl. Med.*, 1975, **16**, 764–768.
32 (*a*) R. Sattos-Oliveira, *et al.*, *Mater. Sci. Eng., C*, 2019, **102**, 405–414; (*b*) M. Wang, *et al.*, *ACS Appl. Mater. Interfaces*, 2017, **9**(49), 42612–42621.
33 X-ray Photoelectron Spectroscopy (XPS) Reference Pages: Gallium, http://www.xpsfitting.com/search/label/Gallium, (accessed 9 February 2020).
34 J. L. Bourque, M. C. Biesinger and K. M. Baines, *Dalton Trans.*, 2016, **45**, 7678–7696.
35 S. Catalán-Gómez, A. Redondo-Cubero, F. J. Palomares, F. Nucciarelli and J. L. Pau, *Nanotechnology*, 2017, **28**, 405705.
36 (*a*) S. Catalán-Gómez, A. Redondo-Cubero, F. J. Palomares, L. Vázquez, E. Nogales, F. Nucciarelli, B. Méndez, N. Gordillo and J. L. Pau, *Nanotechnology*, 2018, **29**, 355707; (*b*) K. Klimova, M. Pumera, J. Luxa, O. Jankovský, D. Sedmidubský, S. Matějková and Z. Sofer, *J. Phys. Chem. C*, 2016, **120**(42), 24203–24212.

